Natural Resources Canada | Ressources naturelles Canada

GEOLOGICAL SURVEY OF CANADA
OPEN FILE 8340

Geochemistry, petrology, and aeromagnetic mapping of the Orpheus dykes, South Rae craton, Northwest Territories

B. Mowbray and S.J. Pehrsson

2019

Canada

GEOLOGICAL SURVEY OF CANADA
OPEN FILE 8340

Geochemistry, petrology, and aeromagnetic mapping of the Orpheus dykes, South Rae craton, Northwest Territories

B. Mowbray[1] and S.J. Pehrsson[2]

[1] Ottawa-Carleton Geoscience Centre, 2115 Herzberg Laboratories, Carleton University, 1125 Colonel By Drive, Ottawa, Ontario K1S 5B6
[2] Geological Survey of Canada, 601 Booth Street, Ottawa, Ontario K1A 0E9

2019

Permanent link: https://doi.org/10.4095/311306

This publication is available for free download through GEOSCAN (http://geoscan.nrcan.gc.ca/).

Recommended citation
Mowbray, B. and Pehrsson, S.J., 2019. Geochemistry, petrology, and aeromagnetic mapping of the Orpheus dykes, South Rae craton, Northwest Territories; Geological Survey of Canada, Open File 8340, 28 p. https://doi.org/10.4095/311306

Publications in this series have not been edited; they are released as submitted by the author.

Abstract

The Orpheus dyke swarm of the South Rae craton in the Northwest Territories is composed of numerous NNE trending, upper amphibolite-granulite facies, metagabbro dykes. The dykes define extensive kilometre long ridges in otherwise flat topography. This work presents the first petrographic and geochemical study of the dykes. We examine possible contamination that occurred during the melt's assent to surface and suggest that geochemically it resembles crustally contaminated EMORB, lending further evidence for extensional events in the Rae in the mid-Paleoproterozoic. The preliminary age of the swarm (*ca*. 2.27 Ga) is unusual in the Canadian Shield but geochemically it shows some similarities to other Paleoproterozoic swarms seen on the Slave craton and Chesterfield Block (Dogrib and Tulemalu respectively). We suggest that the Orpheus swarm was metamorphosed by both the Snowbird and Trans-Hudson Orogenies.

Introduction

This Open File represents the results of a research project undertaken by the first author as part of an undergraduate study at Carleton University in the Winter of 2016. The project focused on understanding the character, petrochemistry and extent of a newly discovered dyke swarm in the South Rae craton of Northwest Territories. A single dyke at Orpheus Lake was first noted by Hoadley (1955). Unpublished map manuscripts of F.D. Taylor from 1955-1957 Operation Thelon showed a dyke swarm just north of Orpheus Lake, but these were subsequently omitted from the published maps (Taylor, 1959). Regional reconnaissance and more detailed mapping by the Geoscience for Energy and Minerals Program in South Rae craton during 2012 and 2015 confirmed the presence of the swarm (Davis et al., 2014, Pehrsson et al., 2013; 2015). In the following contribution the regional context of the dykes, their petrography, distribution and geochemistry are presented and discussed. Geochemical analyses and aeromagnetic interpretations of the dyke distribution are presented in the Additional Data section. A comparison of the Orpheus swarm with other similar Paleoproterozoic swarms such as the Malley, Dogrib and Tulemalu dykes of the Slave craton and Chesterfield Block has been incorporated in order to show the possible similarities in source,.

Background geology of the Orpheus Swarm

The study area lies within the South Rae craton of the Northwest Territories (Fig. 1). The area has been regionally mapped twice, first in the 1950s at 1:500,000 scale (Hoadley, 1955, Taylor, 1957) and second in 2012-15 at 1:250,000 scale (Pehrsson et al., 2016). Samples for this study were taken from two dykes, one identified in 2012 and one in 2015. The dykes as mapped are up to 90 m wide and extend for kilometres, often picked out as topographic ridges trending north- south. They are clearly visible on aeromagnetic data (Fig. A1a,b) and a number of additional dykes have been identified in this study based on the results of a regional aeromagnetic study by Kiss and Coyle (2012; Fig.2).

In outcrop the dykes display a variety of textures. Away from more strongly foliated domains, the dykes are granoblastic with a locally prominent coronitic M1 texture of plagioclase, clinopyroxene and garnet surrounding large clinopyroxene phenocrysts. Local ultramafic clinopyroxene-orthopyroxene segregations are distinctly sulphidic and carry pyrrhotite and chalcopyrite. Centimeter to decimetre scale compositional layering has formed due to metamorphic differentiation and at one site subparallels a grain shape fabric defined by clinopyroxene-orthopyroxene and -plagioclase. This fabric trends west-northwest, at an oblique angle to the regional foliation in the host gneisses and is steeper (60-80 degree south dip). It also carries a prominent stretching lineation defined by clinopyroxene and plagioclase that plunge southeast at 50 degrees. A finer overall modal grain size was noted on the east margin of one dyke, suggestive of original chilled margins.

The Orpheus dykes intrude the Paleoproterozoic McCann granulite domain, a northeast trending region of relatively smooth, low magnetic character (Pehrsson et al., 2016; Fig. 3). The predominant host rocks include Neoarchean to earliest Paleoproterozoic megacrystic orthopyroxene monzogranite, orthopyroxene-garnet paragneiss, diatexite and migmatite (Davis et al., 2015). The latter include rare iron formation and metawacke inclusions. The McCann domain is bounded by the Black Bay fault zone on the east and the Howard Lake-Penylan fault system to the west (Percival et al., 2016). The northwest-trending regional foliation in the domain is defined by granulite facies assemblages dated by monazite and zircon and crosscutting intrusions to be part of the Arrowsmith Orogeny, a major 2.4-2.3 Ga high temperature, moderate to low pressure tectonometamorphic event that affects the western margin of Rae craton (Berman et al, 2013; Regis et al., 2017).

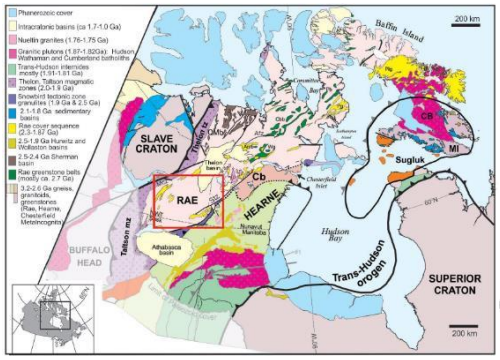

Figure 1. Regional geological map of northwest Laurentia. Area of Figure 2 highlighted by red box. Ab-breviations: Amb = Amer belt; Afz = Amer fault zone, Cb = Chesterfield block, Cbb = Committee Bay belt; CB = Cumberland batholith; Cfz = Mcf = McDonough fault, MI = Meta Incognita; Pb - Prince Albert Group, Pg = Pehnryn Group; Plg = Piling Group; QMb = Queen Maud block, Stz = Snowbird tectonic zone, Thelon tz = Thelon tectonic zone; Wg=Woodburn Group (Davis et. al. 2015).

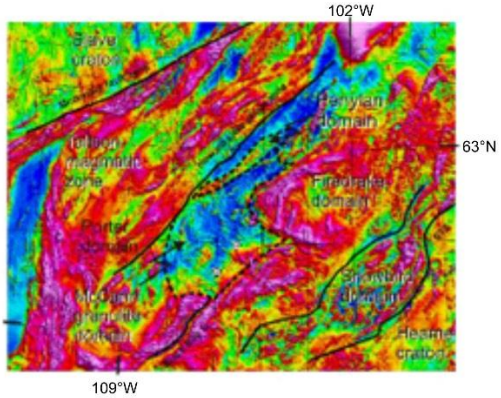

Figure 2. Map of the southern Rae craton showing regional aeromagnetic coverage and boundaries of principal tectonic domains (Pehrsson et al., in press). Locations of samples in this study are shown and identified by sample number. Abbreviations: STZ- Snowbird Tectonic zone; fz = fault zone. (modified from Davis et. al. 2015).

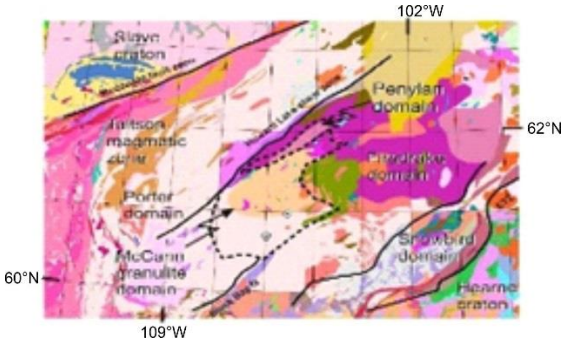

Figure 3. Bedrock compellation geology map (Pehrsson et. al. 2013) of the southern Rae craton showing regional geologic units and boundaries of principal tectonic domains. Locations of samples in this study are shown and identified by sample number. Abbreviations: STZ-Snowbird Tectonic zone; fz = fault zone. (modified from Davis et. al. 2015).

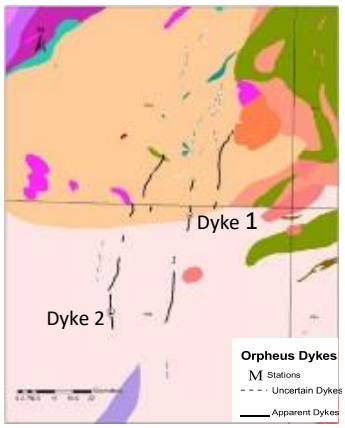

Figure 4. Map of the Orpheus dykes against units of the McCann granulite domain (light orange; modified from Pehrsson et al. 2013).

.

Based on the cross cutting relationships documented by Pehrsson et al (2015) and the age of McCann domain regional foliation (Davis et al., 2013), the maximum age of the Orpheus dykes is 2.32 Ga. Their minimum age is ca. 1.817 Ga, the age of an unmetamorphosed southeast-trending Sparrow diabase dyke that was observed to crosscut dyke 1. U-Pb baddeleyite and igneous zircon dating by M. Hamilton (pers. comm) returns a crystallization age of ca. 2.27 Ga for dyke 1. Low Th/U metamorphic zircons associated with retrogression of the clinopyroxene-garnet assemblage to chlorite and biotite, give an age of ca. 1.83 Ga. The age of the peak M1 assemblage is interpreted to be ca. 1.9 Ga based on a hornblende Ar-Ar cooling age from the immediate dyke 1 wall rocks of the McCann domain (Regis and Kellet, in press).

Method and analytical techniques

Aeromagnetic mapping

The Orpheus dykes were mapped (using ArcGIS 10.2 and/or 10.3) mainly from aeromagnetic data. As noted only two dykes have been visited in outcrop (Fig. 4), and they provide ground truthing for the nature of the prominent north-south, highly magnetic geophysical anomalies traced over the study area. Other strongly magnetised features (i.e. the Mackenzie dykes, Lecheminant and Heaman, 1989) cross-cut and obscure data. To minimise interference, derivatives of the aeromagnetic data were used (Additional Figs A2-7). Uncertain dykes have been marked (dashed lines) in addition to more evident dykes (solid lines) to provide the opportunity to check features in future work. The work herein was compared with a compilation of diabase dykes put together by Buchan and Ernst (2013) and was found to agree largely with their mapping of the swarm.

Petrography

Samples were collected from fresh portions of outcrop in order to characterize the composition, texture, alteration and metamorphic grade of the dykes. Care was taken to avoid to sampling from obscure contacts, heavily altered or retrograded areas. A total of 9 samples were collected from three sites on two dykes (Fig. 4). Of the representative samples examined: one was from site one, four from site two and four from site three. Sites one and two are from northern and

southern extents of dyke 1, while site three is from dyke two. Petrographic via microscopy analysis was performed to examine mineralogy, preservation of igneous textures, and state of deformation.

Geochemistry

For bulk rock geochemistry, weathered surfaces and veins were removed with a rock saw prior to analysis. The sawn samples were crushed into ~5 mm chips using a steel jaw crusher and powdered in an agate mortar. All geochemical analysis was performed by ALS Minerals, Sudbury, Ontario, Canada (http://www.alsglobal.com/en/Our-Services/Minerals/Geochemistry/Downloads). Twelve major element oxides were analyzed; initially the prepared sample (0.20 g) is added to lithium metaborate/lithium tetraborate flux (0.90 g), mixed well and fused in a furnace at 1000°C. The resulting melt is then cooled and dissolved in 100 mL of 4% nitric acid/2% hydrochloric acid. This solution is then analysed by ICP-AES and the results are corrected for spectral inter-element interferences (ALS, ME-ICP06, 2006). Loss on ignition (L.O.I.) values determined by thermal decomposition is also displayed. For 42 elements, including large ion lithophile elements (LILE), high field strength elements (HFSE), rare earth elements (REE), and other trace elements were determined by Inductively Coupled Plasma - Mass Spectrometry (ICP-MS, ALS MES81, 2009). Matrix matching standards TDB1 was run as reference material. Mineral compositions and bulk-rock geochemical data for representative samples are discussed below and presented in Table A1

Results

Mapping

Based on the method outlined, the Orpheus swarm extends in a roughly north-northeast- orientation across the McCann granulite domain for over 80 km, from near Coventry Lake to the Labyrinth River. The swarm does not cross the Black bay fault zone in the south nor the boundary of the McCann and Firedrake domains in the Rennie Lake area. (Figs. 4, A1a, b, A2a, b) At least three major dykes and or dyke segments can be outlined, along with numerous smaller segments, however due to interference the latter interpretations are less uncertain. The dykes display a slightly irregular shape, characterized by undulations about roughly west-northwest axes. Given the orientation of internal fabric in the dykes, it is possible that these undulations represent map scale folding of the dykes, to which the fabric is axial planar.

Petrography

In outcrop the Orpheus dykes show a light grey weathered surface (Fig. 5a, b) , dark green to black pyroxene grains are a distinguishing feature and range from 2 mm to 10 mm (Fig. 5c-d),and large cm scale plagioclase xenoliths are locally present (Fig. 5e-g). Red Mg/Fe-rich garnet is found throughout (Fig. 5h).

In thin section the two dykes are uniform in their mineralogy however they show variable degrees of retrograde metamorphism. Predominantly composed of plagioclase, garnet, and clinopyroxene with lesser amounts of amphibole, biotite and quartz. An oxide (magnetite) is present as an accessory phase. Primary igneous textures are pseudomorphed by peak metamorphic assemblages with retrograde metamorphic minerals replaced the pre-existing fabrics (Fig. 6e-g). Relic plagioclase exists with primary polysynthetic lamination (Fig. 7f) in addition to deformed plagioclase laths (Fig. 7g-h) Plagioclases seen in figure 8c are severely kaolinised. Pyroxenes and plagioclase often form a meta ophitic to subophitic texture while at places clinopyroxene occurs as an interstitial phase amidst euhedral laths of plagioclase (Fig. 7c-d). Amphibole is present in several types (Fig. 7a, 8a-b), iron-rich euhedral grains notably form around oxide mineralisation (Fig. 6h, 8d) while sodic-calcic anhedral amphibole (actinolite) grains appear as pseudomorphs of clinopyroxene (Fig. 6d-g, 7b, 8e-f).

Garnet is a significant component of the mineralogy, forming as coronas around distinct new grains of clinopyroxene (Fig. 6d), as well as in a contact with hornblende. The sample suite exhibits several different types of coronae; thin rims of garnet form around clinopyroxene or plagioclase (Fig. 6c-g, 7d, f, 8e-f), and hornblende forms rims around oxides (Fig. 6h, 8d). The garnet-clinopyroxene coronae around primary clinopyroxene and plagioclase are interpreted to have formed from prograde high temperature metamorphism at minimum conditions of ca. 8 kbar. through the reaction cpx + pl = grt + quartz. Hornblende appears to act as a symplectite replacement reaction (Fig. 7e) filling in structural weakness with clinopyroxene.

Minor amounts of chlorite are present as a retrograde mineral and is fibrous in nature being weakly pleochroic green, inferred to be an alteration product of amphibole.

Figure 5. The Orpheus dykes (a-b) outcrop photos with pen and rock hammer respectively. (c-d) garnet and clinopyroxene in outcrop, stylus for scale. (e-g) plagioclase xenoliths bruton and sharpie for scale. (h) Phenocryst of garnet compass for scale.

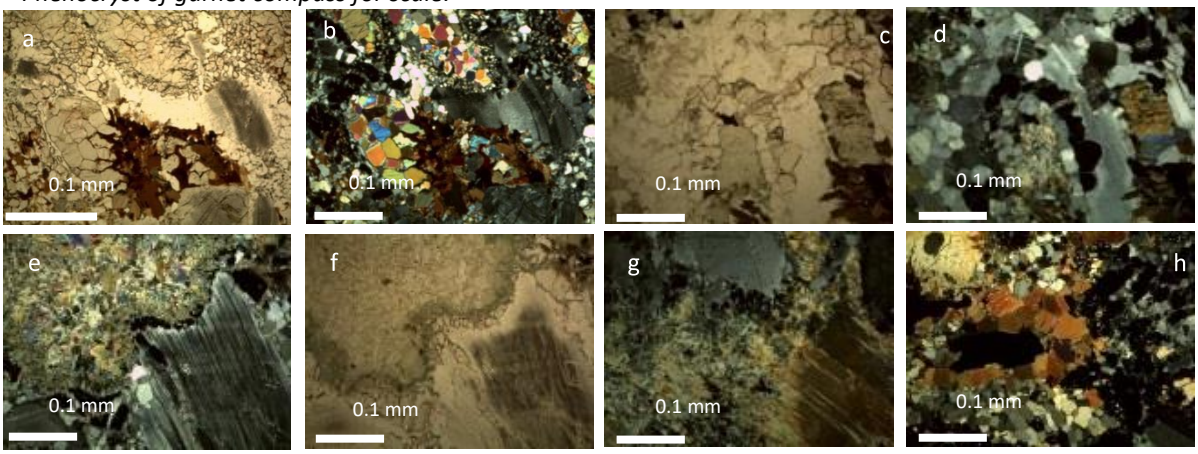

Figure 6. Thin section photos (a-b) amphibole with garnet coronae and biotite growth from amphibole. (c-d) double coronae of garnet and plagioclase around actinolite pseudomorph of clinopyroxene (e-f) coronae of garnet around actinolite pseudomorph of clinopyroxene, on interior of clinopyroxene larger hornblende (g) clinopyroxene and actinolite pseudomorph (h) Hornblende coronae around oxide.

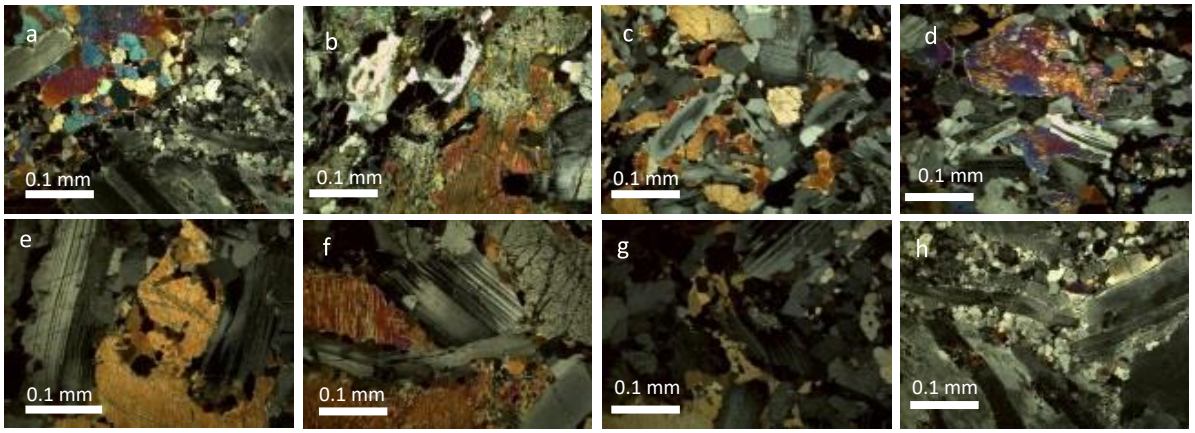

Figure 7. Thin section photos (a) hornblende with garnet coronae. (b) clinopyroxene and actinolite pseudomorph, showing garnet corona (c-d) Clinopyroxene within a ground mass of plagioclase laths (e) symplectite growth of hornblende into clinopyroxene. (f-h) deformation of plagioclase.

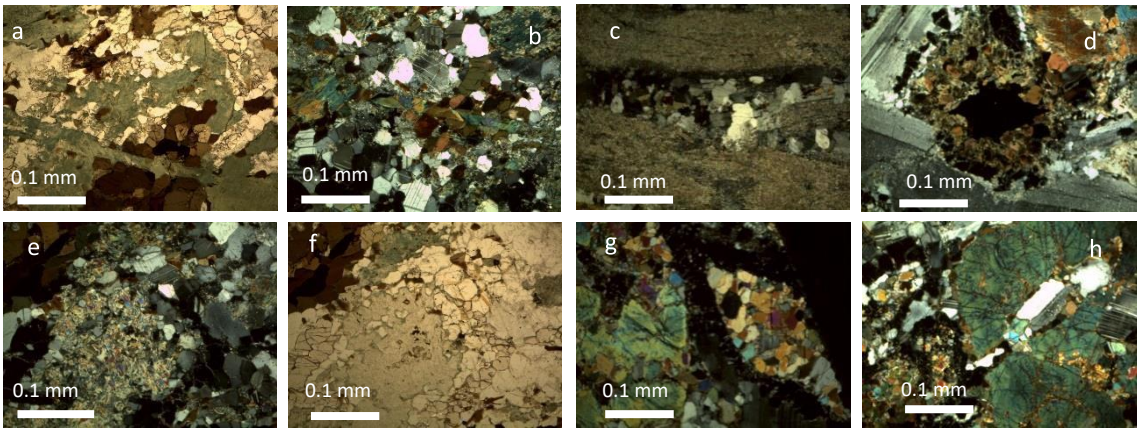

Figure 8. Thin section photos (a-b) amphibole showing Fe-rich and more calcic-sodic characteristics (c) kaolinised plagioclase (d) hornblnde corona around oxide, hornblende plagioclase interaction develops garnets. (e-f) actinolite pseudomorph of clinopyroxene exhibiting double plagioclase/garnet corona (h-g) hornblende – garner coronae.

Geochemistry

Bulk rock geochemistry was conducted on available samples with the intent of determining the geochemical characteristics of the two dykes. Results are presented in Figures 9 to 17. As the dykes are metamorphosed consideration must be given to the affect of this on major and trace element concentrations. A number of studies of metamorphism at differing grades have shown that large ion lithophile elements (LILE; Cs, Na, K, Rb, Ba, Ca, Pb and Sr) can be mobile during metamorphism (Winchester and Floyd, 1977; Polat et al., 2002; Manikyamba et al. 2015). Given the relative immobility of rare earth elements, high field strength elements and transition metals (Polat et al., 2002), along with observed covariation in major element oxides (Fig. 9-13) , it is interpreted that the discriminant diagrams used here are valid for the Orpheus swarm

Major elements

The major element data show that these samples contain SiO2 wt. % of ~48%, MgO wt. % between 5.72 and 8.35 and Na2O and K2O (alkali elements) between 0.48 and 3.18 wt. % (Table A1). The dykes also contain between 15.4 to 17.55 wt. % Al_2O_3, 12.35 to 14.8 wt.% Fe_2O_3, 8.96 and 9.64 wt. % CaO, and <1 wt. % MnO, and <2 wt.% TiO_2. The Orpheus swarm is broadly tholeiitic basalts in composition, plotted on AFM, total alkali-silica and Zr/Ti versus Nb/Y discriminant diagrams (Fig 9-11). CaO/Al_2O_3, SiO_2 and Na_2O demonstrate a negative relationship with MgO; Fe_2O_3 is has weak

positive relation while Al_2O_3 has no evident association; TiO_2 shows a separation of ~0.028 wt. % between the two sampled dykes (Fig. 12). SiO_2, and N_2O outline a negative correlation with Mg # (Fig. 13) while P_20_5 illustrates a compositional difference of ~1.5 Mg# and 0.03 wt. % between the two dykes;. Al_2O_3, Fe_2O_3 K_2O, TiO2, and MnO do not show any obvious correlation with Mg# (Fig. 13).

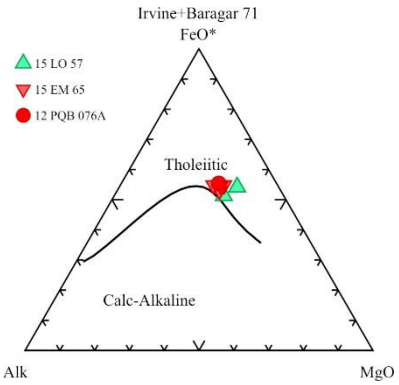

Figure 9. Tertiary plot of FeO, Alk and MgO (AFM) for the Orpheus swarm (after Irvine and Baragar 1971).

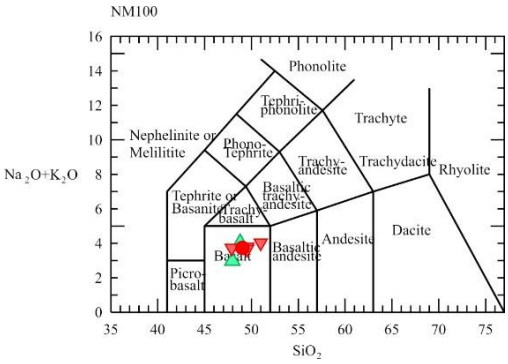

Figure 10. Total alkali vs. silica (TAS) diagram showing the plots for Orpheus swarm (after Le Bas et. al. (1986).

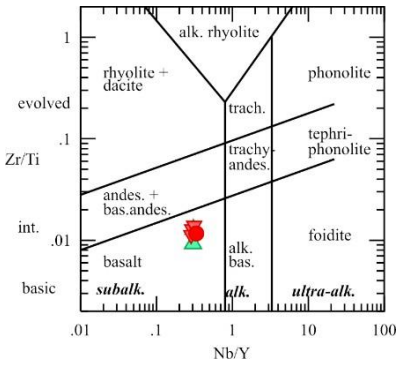

Figure 11. bivariate Zr/Ti vs Nb/Y diagram for the Orpheus swarm (after Winchester and Floyd 1977; Pearce 1996).

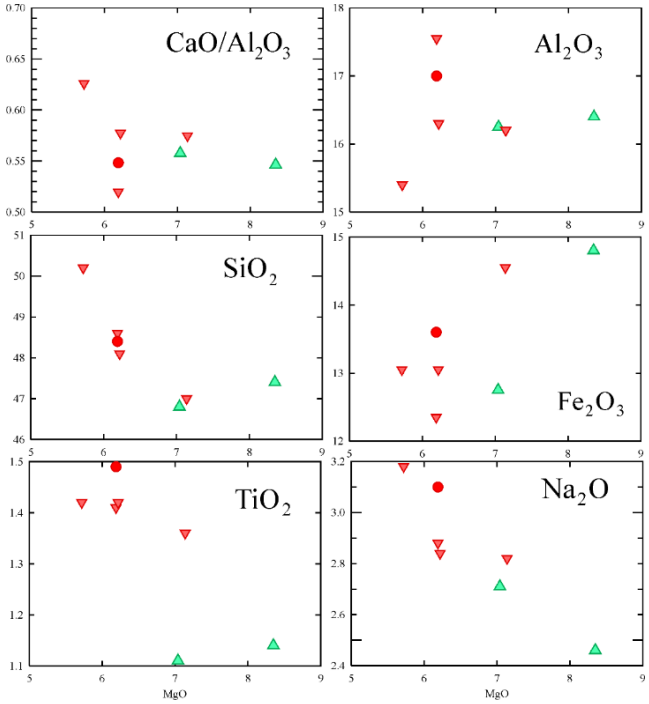

Figure 12. Major elements vs. MgO plot for the Orpheus swarm. Symbols per Figure 9.

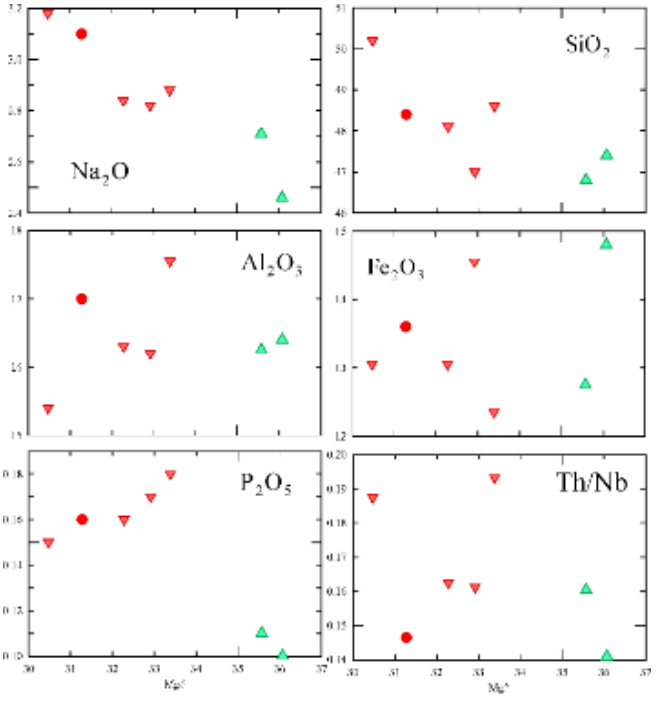

Figure 13. Major elements vs. Mg# plot for the Orpheus swarm. Symbols per Figure 9.

Trace element composition:

Normalized trace element plots of Orpheus samples REE (rare earth element) and trace element abundances are presented in Figures 14 to 17. Trace element abundances range from 2 to 40 times those in MORB (Fig. 14, Pearce, 1983); 5 to 1000 times that of primitive mantle (PM, (Fig. 15, Sun and McDonough, 1989) and 5 to 100 times the abundance of EMORB (Fig.16, ibid) 10 to 60 times the abundances of chondrite (Fig. 14-17, ibid). The LREE (light rare earth elements) are far more enriched than are the HREE (heavy rare earth elements), with a relatively steady negative slope from lanthanum (La) to lutetium (Lu) (Fig.. 16,17). All samples show the same trend however dyke 2 has notably lower abundances.. When plotted against MORB, samples from both dykes show significant enrichment in Rb, Ba, Th and Ce while having a depleted abundance of Zr, Hf, Ti, Y and Yb (Fig. 14; Pearce 1983). Samples 15 LO 57A and 12PQB 076A show a distinct spike in Rb, and Th respectively, then follow the same negative trend to Yb as the rest of the samples. Seen in data normalized to PM and EMORB the Orpheus samples exhibit positive K and Pb and Nd as well as negative Nb, and P anomalies, relative to neighbouring HFSE and REE. Orpheus Th/Yb trends are high and just above the EMORB field of basalt Pearce (2008) discrimination diagram

.

Discussion:

Petrogenesis and Melt Contamination

The Orpheus dykes are uniformly tholeiitic (Fig. 9) and exclusively within the basaltic range of figure 10, and 11 (Le Bas et.al. 1986; Winchester and Floyd 1977; Pearce 1996 respectively). The dykes exhibit a Th/Yb trend (Fig. 18, 19) (Pearce 2008) and anomalously high trace element concentrations of Pb, possibly indicate metamorphic remobilization. Nd is somewhat high and Nb concentrations are somewhat low (Fig. 14, 15, 16) (Pearce 1983; Sun and McDonough 1989 respectively). The trends could imply contamination of the melt; either as the magma traveled through silicic continental crust or as it traveled through enriched mantle lithosphere (Pearce 2008), resulting in an apparently crustal signature. This is supported by the high Nd trace element compositions that are widely interpreted as the consequence of selective contamination of the magmas (Huppert et. al. 1985). Negative Nb could be attained as melt traveled through lower mantle lithosphere (Ernst and Buchan, 2010).

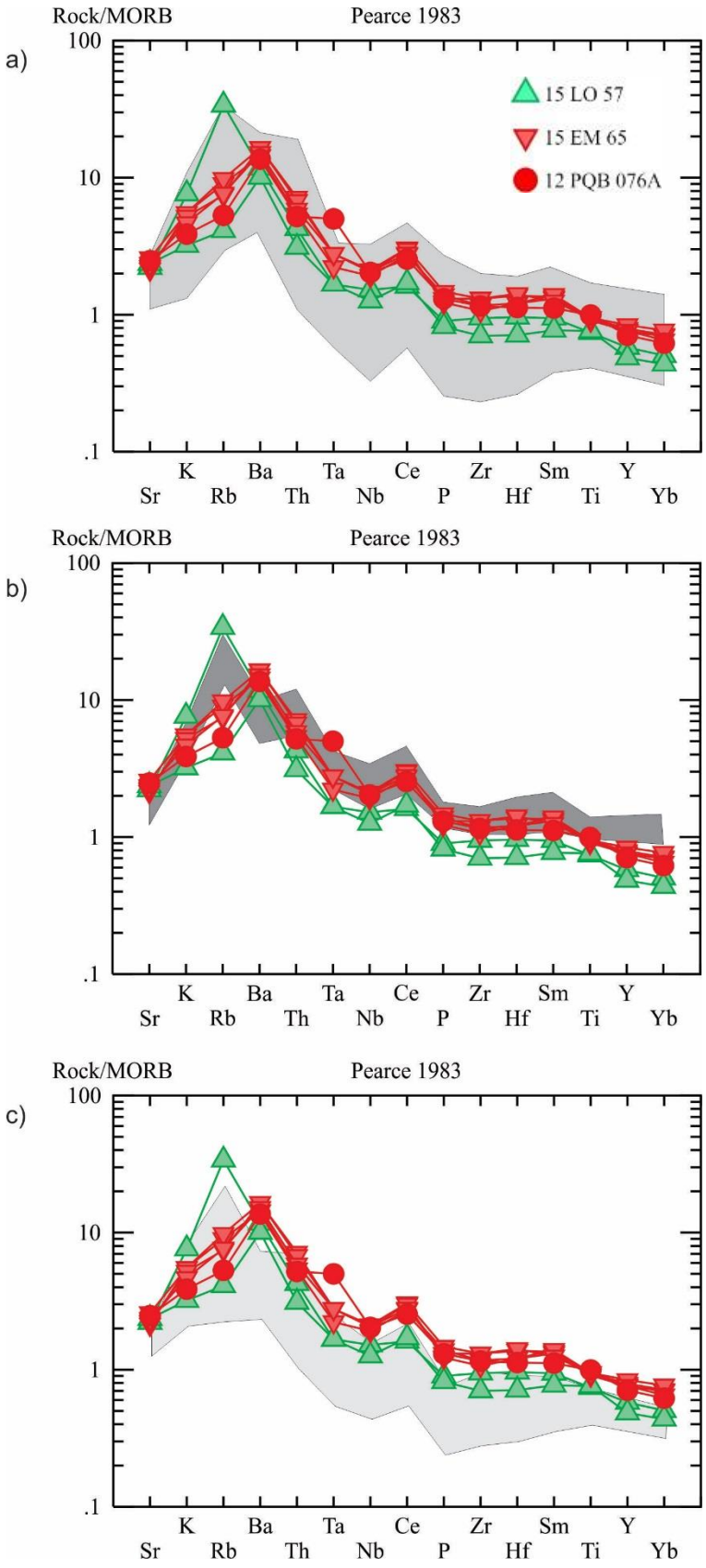

Figure 14. Orpheus dykes MORB normalised (after Pearce 1983); a), b), c), plotted against fields in grey for Tulemalu, Malley, and Dogrib respectively.

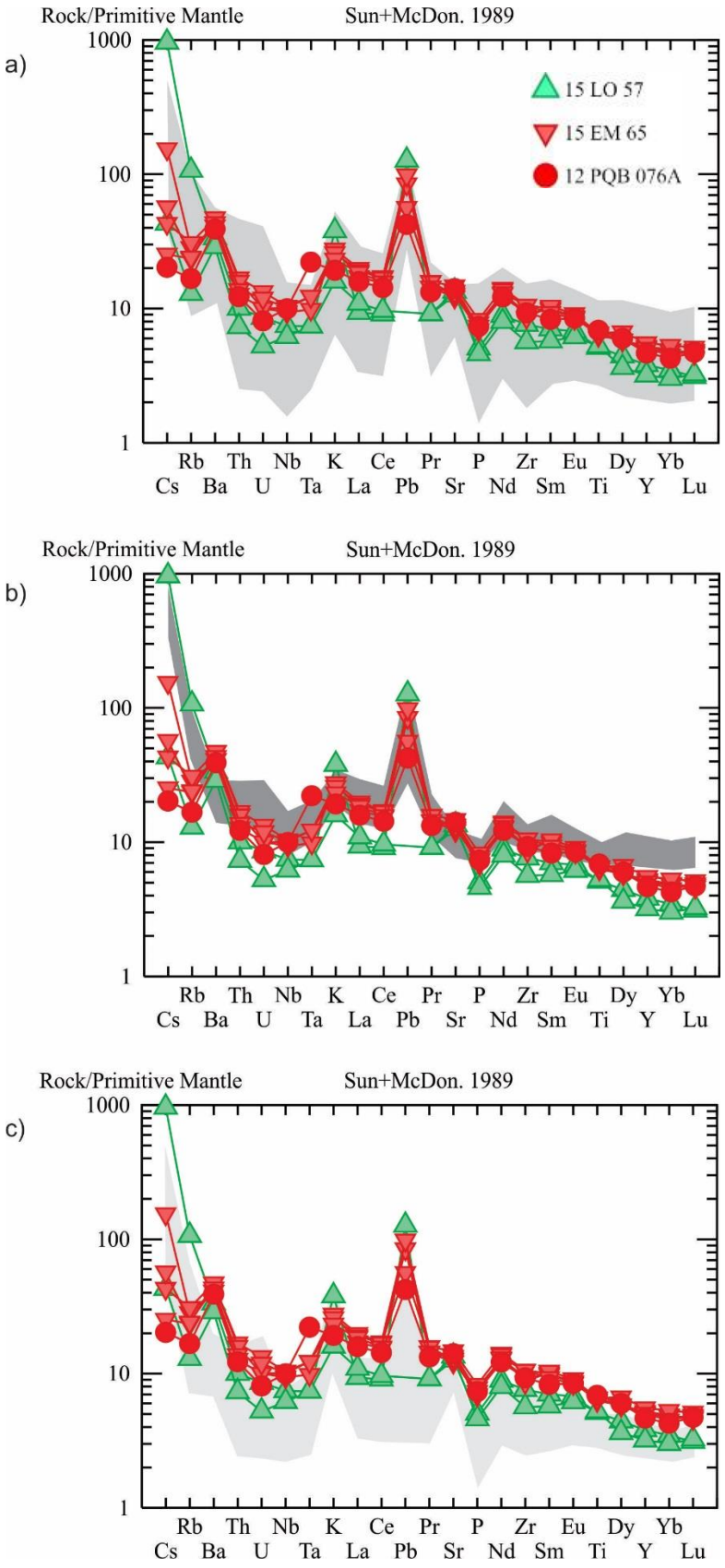

Figure 15. Orpheus dykes PM normalised (after Sun and McDonough 1989); a), b), c), plotted against fields in grey for Tulemalu, Malley, and Dogrib respectively.

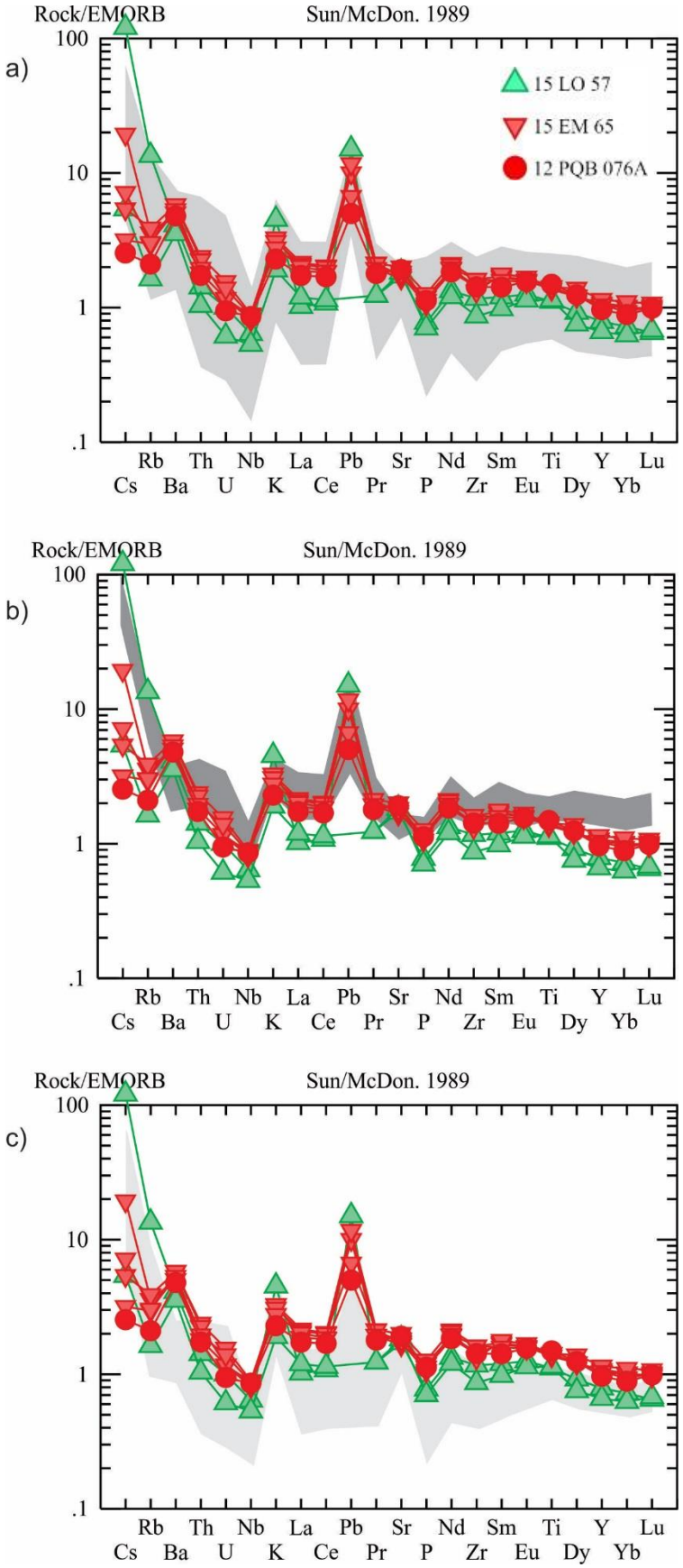

Figure 16. Orpheus dykes EMORB normalised (after Sun and McDonough 1989). a), b), c), plotted against fields in grey for Tulemalu, Malley, and Dogrib respectively.

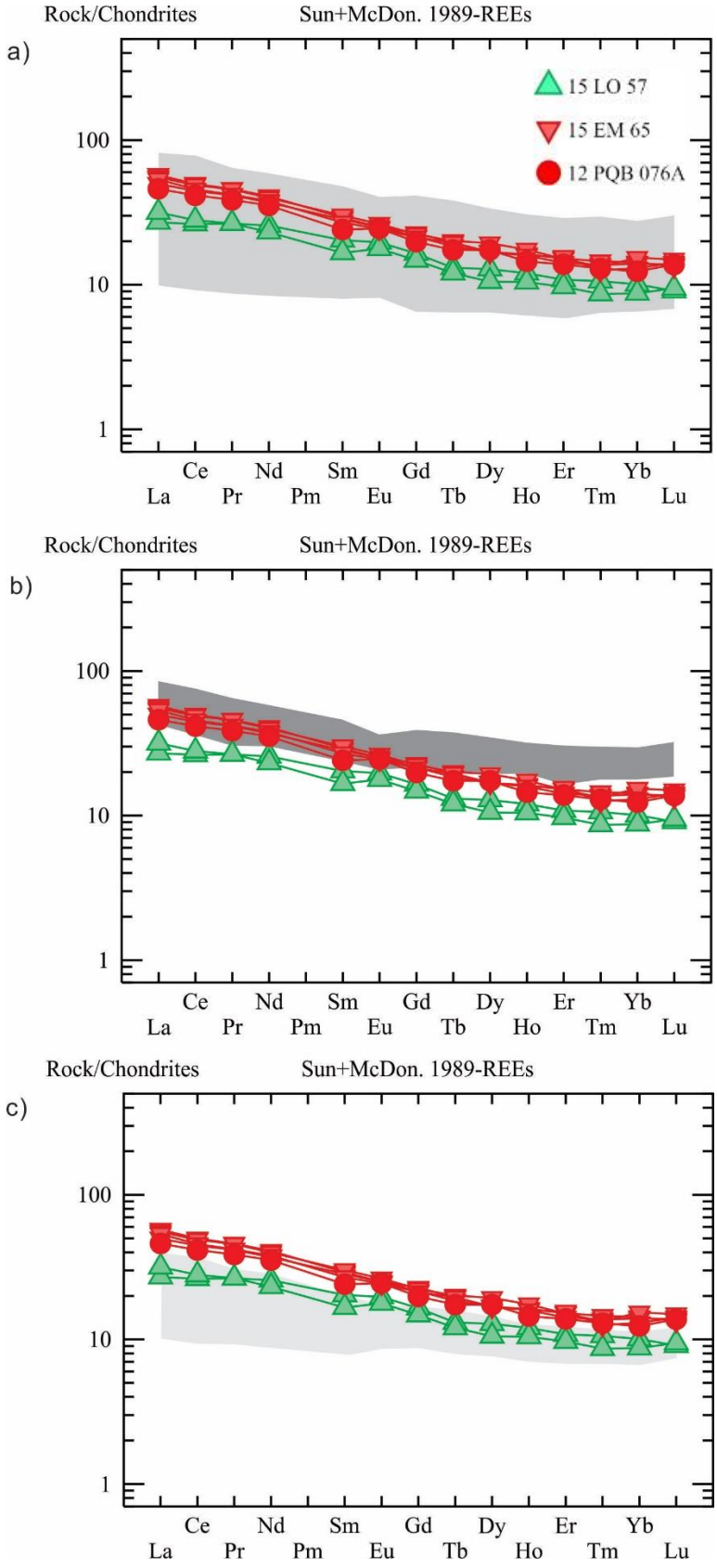

Figure 17. Orpheus dykes REEs chondrite normalised (after Sun and McDonough 1989); a), b), c), plotted against Tulemalu, Malley, and Dogrib fields in grey respectively.

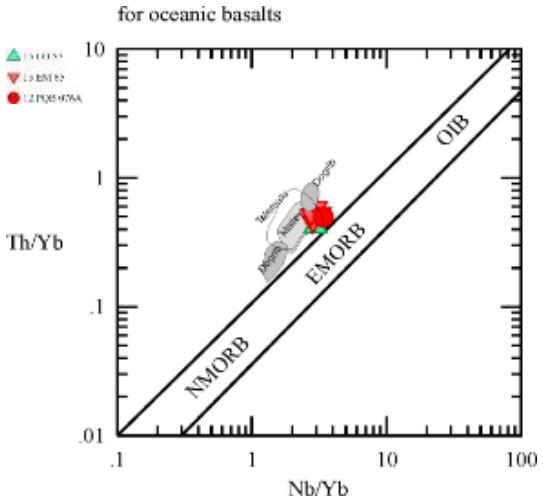

Figure 18. Th/Yb vs. Nb/Yb diagram that illustrat9es the input of Th from either crustal contamination (CC) or subduction zone flux.

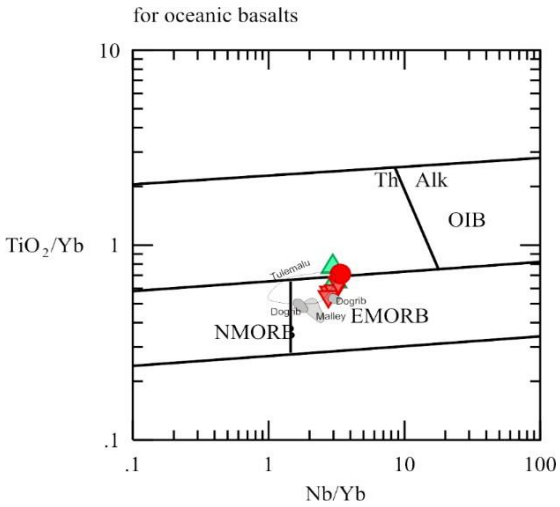

Figure 19. Ti/Yb vs. Nb/Yb diagram for the Orpehus swarm.

Geochemical Comparisons

The Orpheus dykes have been compared herein with geochemical data collected by Ernst and Buchan (2010) for swarms of a broadly similar age within the Slave craton and Chesterfield Block (CB). U-Pb baddeleyite ages of 2.19 Ga have been determined for ENE-striking Dogrib dykes in the Slave craton and for E-striking Tulemalu dykes in the Yathkyed and MacQuoid belts of CB (Fahrig et al, 1984). The NE-trending Malley dyke swarm of the slave craton has an age of 2.23 Ga (U-baddeleyite; Buchan et. al. 2012). Individual melting characteristics are discussed below.

The individual swarms: Tulemalu (CB), Dogrib and Malley (Slave) each have unique melt characteristics that distinguish their distinctive histories. Through trace element and REE data, the Tulemalu dykes illustrate a weak similarity to the Orpheus swarm. Elements Th and U have distinct peaks in MORB, PM and EMORB normalized data that are that not present in the Orpheus. The Malley dykes do not illustrate the negative slope in HREE that marks Orpheus data (Fig. 17);

additionally, the Malley has peaks of Th and U. The Data for the Dogrib exhibits enrichment in Rb, Th and Ce while having a depleted abundance of Zr, Hf, Ti, Y and Yb (Fig.s 14-17). Data exhibit positive K and Pb and Nd as well as negative Nb, and P anomalies, relative to neighbouring HFSE and REE. The trends exhibited by the Dogrib swarm demonstrate a broadly similar geochemical signature to that of the Orpheus. Trends seen between the Dogrib, Tulemalu and Orpheus suggest a generally similar melt evolution, typical of contamination for dyke swarms during continental rifting. It is important to note that even though geochemistry is similar it only represents the evolution of melt for the individual dykes.

There are presently no well dated dyke swarms to fall in the age range of ca 2.3-2.24 Ga (Buchan et al., 2013), and key time in earth evolution (Pehrsson et al., 2014), making the Orpheus dykes somewhat unique. They were emplaced just after the Arrowsmith orogeny (Berman et al., 2013) and overlap with the onset of extension and cover sequence sedimentation across the Rae (Rainbird et al., 2010) The Orpheus swarm may have been emplaced as a crustally contaminated EMORB formed as part of an attempted rifting episode of the South Rae craton, contemporaneous with early post Arrowsmith sedimentation.

Tectonic implication of metamorphism

The Orpheus dykes record the affects of two tectonometamrphic events: an M1 peak assemblage and associated deformation and an M2 retrograde metamorphic assemblage. These are bracketed between ca 2.27 Ga and 1.83 Ga. As discussed above, given hornblende Ar-Ar cooling ages in the adjacent units, the M1 peak garnet-clinopyroxene assemblage must be ca. 1.9 Ga in age. This allows it to possibly be related to either the 1.95-1.92 Ga Thelon or 1.90-1.88 Ga Snowbird orogenies (Berman et al., 2007). Given that there are no known high pressure rocks of Thelon orogeny age in the South Rae (Berman et al.2007) but Snowbird age metamorphism and high pressure is well documented (ibid; Martel et al., 2008) , it seems most likely that M1 is a Snowbird orogenic event. The subsequent replacement of clinopyroxene by hornblende and actinolite indicates that relate to post peak M2 amphibolite-greenschist conditions are considered to be related to the Trans-Hudson orogen, which overlaps in age with the metamorphic zircon rims on baddeleyite in the dykes (M. Hamilton, pers. comm.).

Summary and conclusions:

1. Aeromagnetic mapping is an effective tool for tracing the extent of the Orpheus dykes and has provided an aerial extent of > 75 km of length to the NNE striking swarm.
2. Rocks of the Orpheus swarm are metagabbros with grt-cpx coronas. Mineral assemblage considerations demonstrated that they have been metamorphosed under upper amphibolite to granulite facies conditions.
3. The Orpheus dykes are uniformly tholeiitic basalts that may have been emplaced as a crustally contaminated EMORB
4. Trends seen between the Dogrib, Tulemalu and Orpheus suggest a broadly similar melt evolution. It is important to note that even though geochemistry is similar it only represents the evolution of melt for the individual dykes.
5. Metamorphic events that effected the Orpheus swarm would have been likely linked to both the Snowbird and Trans-Hudson orogenies.

Acknowledgements

We thank Richard Ernst for supervising the original research project, Sharon Carr and Ian Honsberger for being second readers, and Pedro Acosta-Gongora for a constructive review of this open file. The project would not have been possible without the assistance of the GSC South Rae field crew of 2015, a crew co-lead by Edith Martel and Janet Campbell.

References

ALS Minerals Sudbury, Geochemical Procedure, ME- MS81 Ultra- Trace Level Methods,http://www.alsglobal.com/Our-Services/Minerals/Geochemistry/Downloads, accesed 2016

Aspler, L.B., Chiarenzelli, J.R., 1998. Two Neoarchean supercontinents? Evidence from the Palaeoproterozoic. Sedimentary. Geology. V. 120, p. 75–104

Berman, R.G., Davis, W.J., and Pehrsson, S., 2007. The collisional Snowbird tectonic zone resurrected: growth of Laurentia during the 1.9 Ga accretionary phase of the Trans-Hudson orogeny: Geology, v. 35, p. 911-914

Berman, R. G.; Pehrsson, S.; Davis, W. J.; Ryan, J. J.; Qui, H.;and Ashton, K. E. 2013.
The Arrowsmith orogeny: Geochronological and thermobarometric constraints on its extent and tectonic setting in the Rae craton, with implications for pre-Nuna supercontinent reconstruction. Precambrian Research, v. 232, p. 44-69

Buchan, K. L., LeCheminant, A. N., van Breemen, O. and Mareschal, J.-C. 2012. Malley diabase dykes of the Slave craton, Canadian Shield: U–Pb age, paleomagnetism, and implications for continental reconstructions in the early Paleoproterozoic. Canadian Journal of Earth Sciences, v. 49, p. 435–454

Buchan, K. L. and Ernst, R. E. 2013. Diabase dyke swarms of Nunavut, Northwest Territories and Yukon, Geological Survey of Canada, Open File 7464, 2013, 24 pages (1 sheet),

Davis, W.J., Pehrsson, S.J. and Percival, J.A, 2015. Results of a U-Pb zircon geochronology transect across the southern Rae craton, NWT, Canada: 2009-2014 Geological Survey of Canada, Open File Open File 7655, 74p

Ernst, R. E. and Buchan, K. L. 2010. Geochemical database of Proterozoic intraplate mafic magmatism in Canada. Geological Survey of Canada Open File 6016, 1 CD–ROM

ESRI 2011. ArcGIS Desktop: Release 10. Redlands, CA: Environmental Systems Research Institute

Fahrig, W. F., Christie, K. W., Eade, K. E. and Tella, S. Paleomagnetism of the Tulemalu dykes, Northwest Territories, Canada. Canadian Journal of Earth Sciences, v., 21, p. 544–553 (1984)

Hoadley, J.W. 1955. Abitau Lake, District of Mackenzie, Northwest Territories (map with marginal notes), Geological Survey of Canada Paper 55-10, 1:250,000 scale.

Huppert, H. E., Stephen, R. and Sparks, J. 1985. Cooling and contamination of mafic and ultramafic magmas during ascent through continental crust. Earth and Planetary Science Letters, v. 74, p. 371–386

Irvine, T. N. and Baragar, W. R. A. 1971. A Guide to the Chemical Classification of the Common Volcanic Rocks. Canadian Journal of Earth Science, v. s 8, p. 523–548

Kiss, F. and Coyle, M., 2012. Aeromagnetic survey of the South Rae Craton, Northwest Territories; Geological Survey of Canada, Open File 7120-7136, scale 1:100 000).

LeBas, M. ., LMaitre, R. W., Streckeinsen, A. and Zanettin, B. 1986. A chemical classification of volcanic rocks based on the total alkali silica diagram. Journal of. Petrology, v. 27, p. 745–750

LeCheminant, A. N. and Heaman, L. M. 1989. Mackenzie igneous events, Canada: Middle Proterozoic hotspot magmatism associated with ocean opening. Earth and Planetary Science Letters, v. 96, p. 38–48

Manikyamba , C., Ganguly, S., Santosh, M., Saha, A., and Lakshminarayana, G. 2015, Geochemistry and petrogenesis of Rajahmundry trap basalts of Krishna-Godavari Basin, India. Geoscience Frontiers, v. 6, p. 437-45

Martel, E., van Breemen, O., Berman, R. G. and Pehrsson, S. 2008. Geochronology and tectonometamorphic history of the Snowbird Lake area, Northwest Territories, Canada: New insights into the architecture and significance of the Snowbird tectonic zone. Precambrian Research, v. 161, p. 201–230

Pearce, J.A. 1983. Role of Sub-Continental Lithosphere in Magma Genesis at Active Continental Margins. In Hawkesworth, C.J. and Nurry, M.L., Eds., Continental Basalts and Mantle Xenoliths, Shiva, Nantwich, p. 230-249

Pearce, J.A. 1996. A User's Guide to Basalt Discrimination Diagrams. In Wyman, D.A., Ed., Trace Element Geochemistry of Volcanic Rocks Applications for Massive Sulphide Exploration, Geological Association of Canada, Short Course Notes, Vol. 12, p. 79-113

Pearce, J. A. 2008. Geochemical fingerprinting of oceanic basalts with applications to ophiolite classification and the search for Archean oceanic crust. Lithos, v. 100, p. 14–48

Pehrsson, S.J.; Currie, M.; Ashton, K.E.; Harper, C.T.; Paul, D.; Pana, D.; Berman, R.G.; Bostock, H.; Corkery, T.; Jefferson, C.W.; and Tella, S. 2013. Compilation (1:550,000) - South Rae and parts of Hearne domains, Churchill Province Northwest Territories, Saskatchewan, Nunavut, Manitoba, and Alberta. Geological Survey of Canada, Open File 5744, 3 sheets

Pehrsson**, S**., Buchan, K., Eglington, B., Berman, R., and Rainbird, R., 2014. Did plate tectonics shutdown in the Palaeoproterozoic? A view from the Siderian geologic record. Gondwana Research. v 26, issue 3–4, p. 803–815

Pehrsson, S.J., Campbell, J.E. , Martel, E., McCurdy, M. , Agosta-Gongora, P., Thiessen, E., Jamieson, D., Lauzon, G., Buller, G., Falck, H., and Dyke. A.S. 2015. Report of 2015 Activities for the Geologic and Metallogenic Framework of the South Rae Craton, Southeast NWT: GEM 2 South Rae Quaternary and Bedrock Project; Geological Survey of Canada, Open File 7958. 25p.)

Percival, J A; Martel, E; Pehrsson, S J; Acosta-Gongora, P; Regis, D; Theissen, E; Jamieson, D; Neil, B; and Knox, B; 2016. Report of 2016 bedrock activities for the geologic and metallogenic framework of the south Rae Craton, southeast NWT: GEM 2 South Rae Quaternary and Bedrock Project. Geological Survey of Canada, Open File 8142, 17 p.

Polat, A., Hofmann, A.W., and Rosing, M. 2002, Boninite-like volcanic rocks in the 3.7-3.8 Ga Isua greenstone belt, West Greenland: geochemical evidence of intra-oceanic subduction processes in the early Earth: Chemical Geology, v. 184, p. 231-254

Regis, D; Martel, E; Davis, W J; and Pehrsson, S J; 2017. U-Pb zircon geochronology of metaplutonic rocks across the southern Rae Province, Northwest Territories. Geological Survey of Canada, Open File 8254, 37 p.

Sun, S -s. and McDonough, W. F. 1989. Chemical and isotopic systematics of oceanic basalts: implications for mantle composition and processes. Geological Society, London, Special Publications , v. 42, p. 313–345

Taylor, F.D. 1959. Geology, Penylan Lake - Firedrake Lake, District of Mackenzie, Northwest TerritoriesGeological Survey of Canada. Preliminary Series Map 1959-8, I sheet, 1: 250,000 scale

Winchester, J. A. and Floyd, P. A. 1977. Geochemical discrimination of different magma series and their differentiation products using immobile elements. Chemical Geology, v. 20, p. 325–343.

Appendix A: Analytical and Additional data

Table A1. Raw Geochemistry data (ALS Minerals, Sudbury, Ontario, Canada, http://www.alsglobal.com/en/Our- Services/Minerals/Geochemistry/Downloads). Dyke One on the left (samples: 15LO57 and 12 PQB76) Dyke two on the right (samples EM65).

		15 LO 57A	15 LO 57B	12 PQB 076A	15 EM 65B	15 EM 65C	15 EM 65D	15 EM 65E
Ba	ppm	234	201	273	287	329	330	303
Ce	ppm	16.1	17.1	25.4	27.3	30.5	29.9	27.9
Cr	ppm	150	80	90	90	60	110	120
Cs	ppm	7.58	0.34	0.16	1.22	0.34	0.2	0.45
Dy	ppm	3.26	2.67	4.41	4.29	4.26	4.92	4.29
Er	ppm	1.79	1.6	2.29	2.34	2.51	2.49	2.58
Eu	ppm	1.14	1.03	1.42	1.45	1.45	1.53	1.41
Ga	ppm	18	17.1	19.7	18.6	19.4	20.1	19.8
Gd	ppm	3.38	3.03	4.07	4.43	4.68	4.58	4.36
Hf	ppm	2.3	1.7	2.7	2.9	3.3	2.9	3.4
Ho	ppm	0.68	0.59	0.82	0.9	0.92	0.99	0.9
La	ppm	6.4	7.5	10.9	11.8	13.6	13.1	12.7
Lu	ppm	0.23	0.24	0.35	0.35	0.34	0.38	0.36
Nb	ppm	5.3	4.4	7.1	6.7	7.4	7.2	7.2
Nd	ppm	12	10.8	16.5	17.3	19.1	18.6	17.7
Pr	ppm	2.51	2.52	3.67	3.95	4.37	4.34	3.98
Rb	ppm	67.7	8.2	10.6	18	19.6	14.9	15.3
Sm	ppm	3.11	2.54	3.68	4.33	4.45	4.61	4.12
Sn	ppm	2	1	1	1	1	1	1
Sr	ppm	265	283	297	256	310	267	282
Ta	ppm	0.3	0.3	0.9	0.4	0.5	0.5	0.5
Tb	ppm	0.49	0.45	0.65	0.69	0.73	0.75	0.73
Th	ppm	0.85	0.62	1.04	1.08	1.43	1.35	1.17
Tm	ppm	0.27	0.22	0.33	0.35	0.37	0.34	0.32
U	ppm	0.18	0.11	0.17	0.21	0.28	0.21	0.25
V	ppm	174	142	145	172	161	206	184
W	ppm	1	<1	<1	1	1	<1	1
Y	ppm	17.3	14.5	21.2	22.8	23.7	25.2	22.9
Yb	ppm	1.71	1.48	2.1	2.37	2.42	2.61	2.21
Zr	ppm	85	63	104	105	118	96	118
SiO2	%	46.8	47.4	48.4	47	48.6	50.2	48.1

		15 LO 57A	15 LO 57B	12 PQB 076A	15 EM 65B	15 EM 65C	15 EM 65D	15 EM 65E
Al2O3	%	16.25	16.4	17	16.2	17.55	15.4	16.3
Fe2O3	%	12.75	14.8	13.6	14.55	12.35	13.05	13.05
CaO	%	9.06	8.96	9.32	9.31	9.12	9.64	9.41
MgO	%	7.04	8.35	6.19	7.14	6.19	5.72	6.22
Na2O	%	2.71	2.46	3.1	2.82	2.88	3.18	2.84
K2O	%	1.14	0.48	0.58	0.83	0.83	0.78	0.7
Cr2O3	%	0.02	0.01	0.01	0.01	0.01	0.02	0.02
TiO2	%	1.11	1.14	1.49	1.36	1.41	1.42	1.42
MnO	%	0.18	0.19	0.19	0.2	0.16	0.19	0.18
P2O5	%	0.11	0.1	0.16	0.17	0.18	0.15	0.16
SrO	%	0.03	0.04	0.03	0.03	0.04	0.03	0.03
BaO	%	0.03	0.02	0.03	0.03	0.04	0.04	0.03
LOI	%	0.91	-0.14	-0.01	0.58	0.21	0.17	0.39
Total	%	98.14	100.21	100.09	100.23	99.57	99.99	98.85
Ag	ppm	<0.5	<0.5	<0.5	<0.5	<0.5	<0.5	<0.5
As	ppm	<5	<5	<5	<5	<5	<5	<5
Cd	ppm	0.6	0.5	0.5	0.5	<0.5	<0.5	<0.5
Co	ppm	48	59	44	49	44	39	47
Cu	ppm	30	48	49	35	23	36	42
Li	ppm	30	<10	<10	10	10	10	10
Mo	ppm	<1	1	1	<1	1	<1	1
Ni	ppm	84	115	72	80	83	46	75
Pb	ppm	9	<2	3	6	7	4	7
Sc	ppm	24	21	23	24	18	34	25
Tl	ppm	<10	<10	<10	<10	<10	<10	<10
Zn	ppm	110	116	115	114	112	109	105

Additional Data Figures

In the following figures, each image on left shows the aeromagnetic data without interpretation and image on right shows the same data with interpreted Orpheus dyke traces in black.

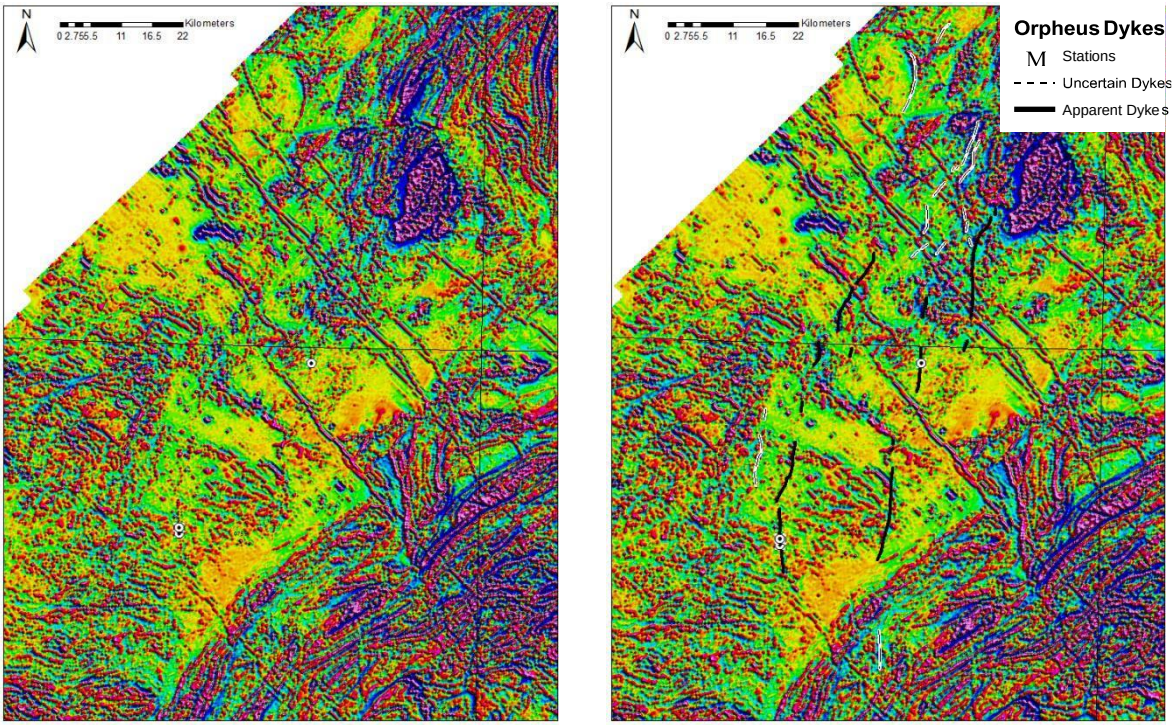

Figure A1a. Map of the Orpheus dykes showing first derivative aeromagnetic coverage at 1:500 000, and A1b, right, with interpretation

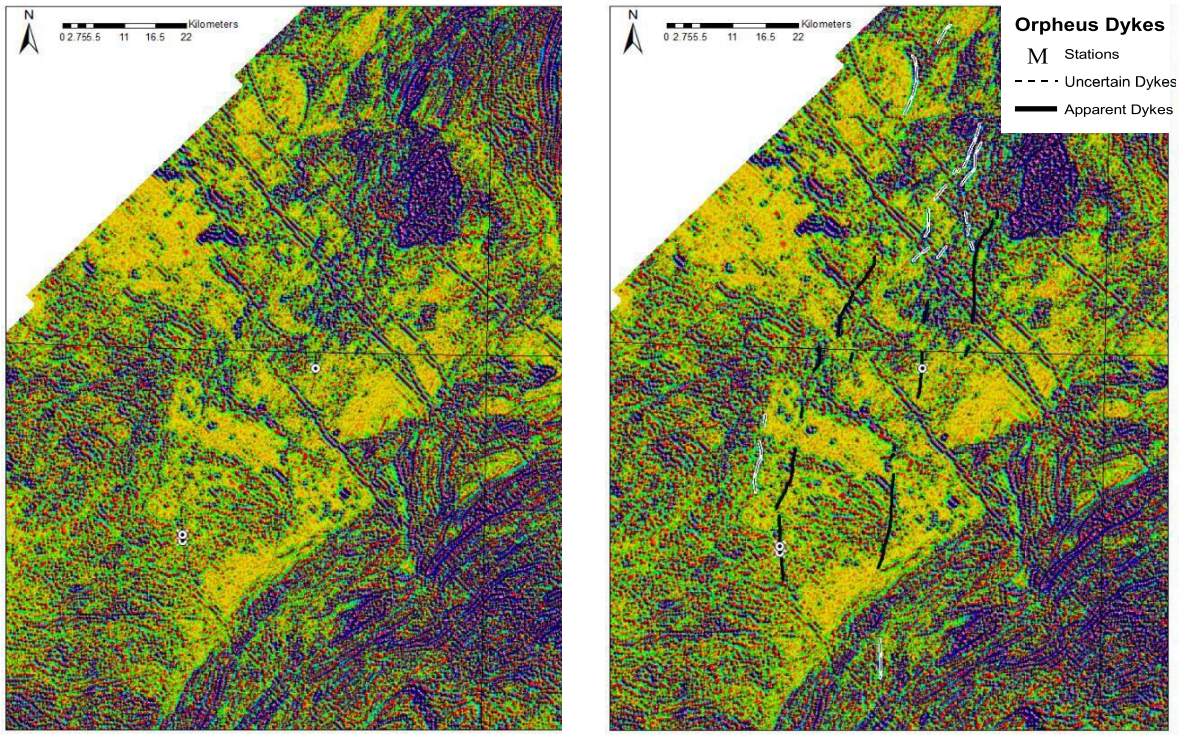

Figure A2a. Map of the Orpheus dykes showing second derivative aeromagnetic coverage at 1:500 000, and A2b, right, with interpretation

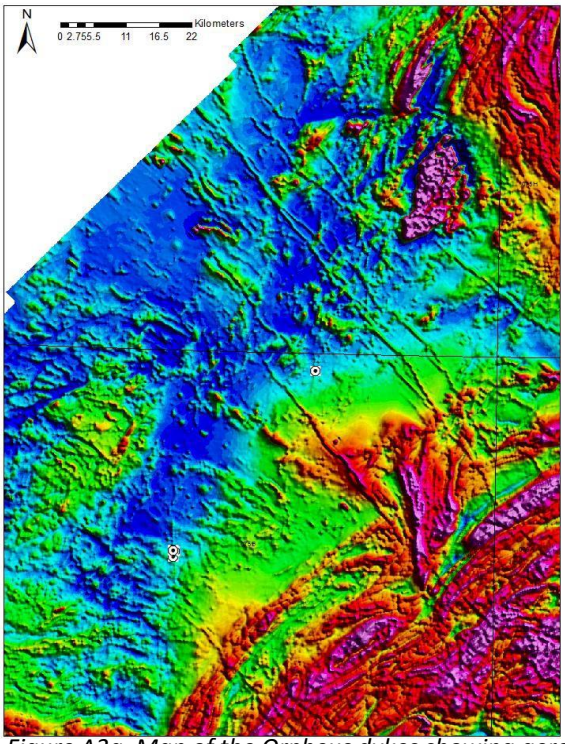

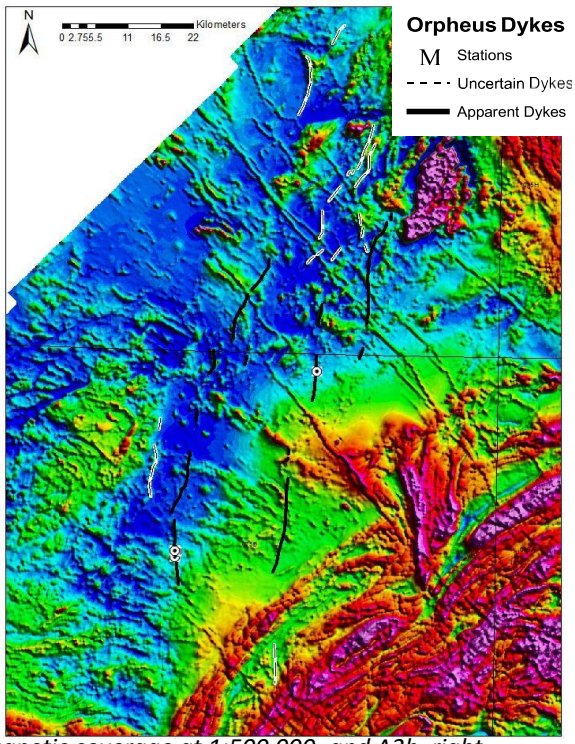

Figure A3a. Map of the Orpheus dykes showing aeromagnetic coverage at 1:500 000, and A3b, right, with interpretation

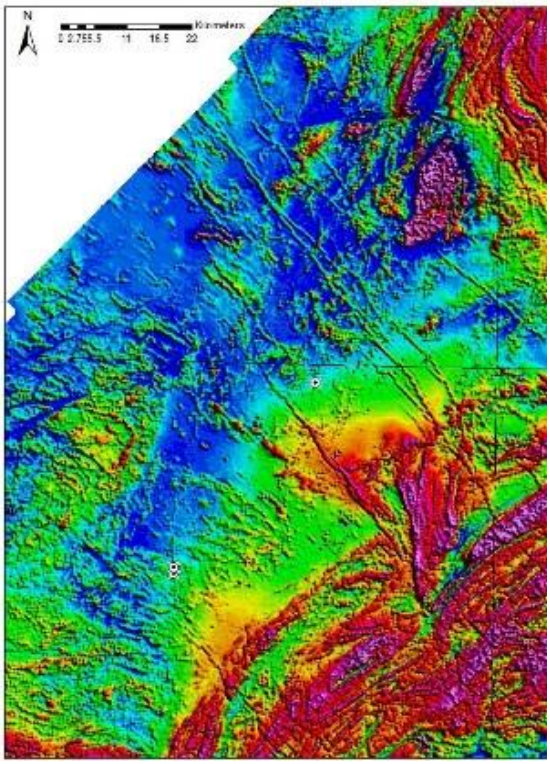

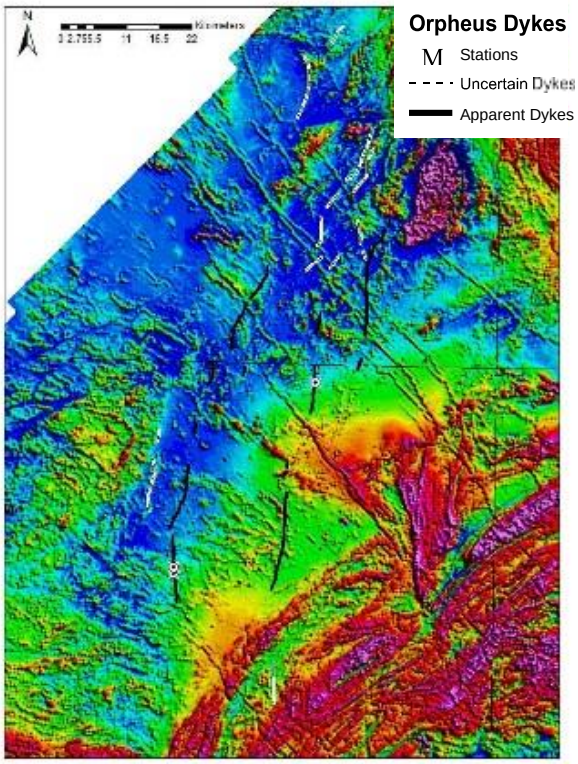

Figure A4a. Map of the Orpheus dykes showing magnetic susceptibility aeromagnetic coverage at 1:500 000, and A4b, right, with interpretation

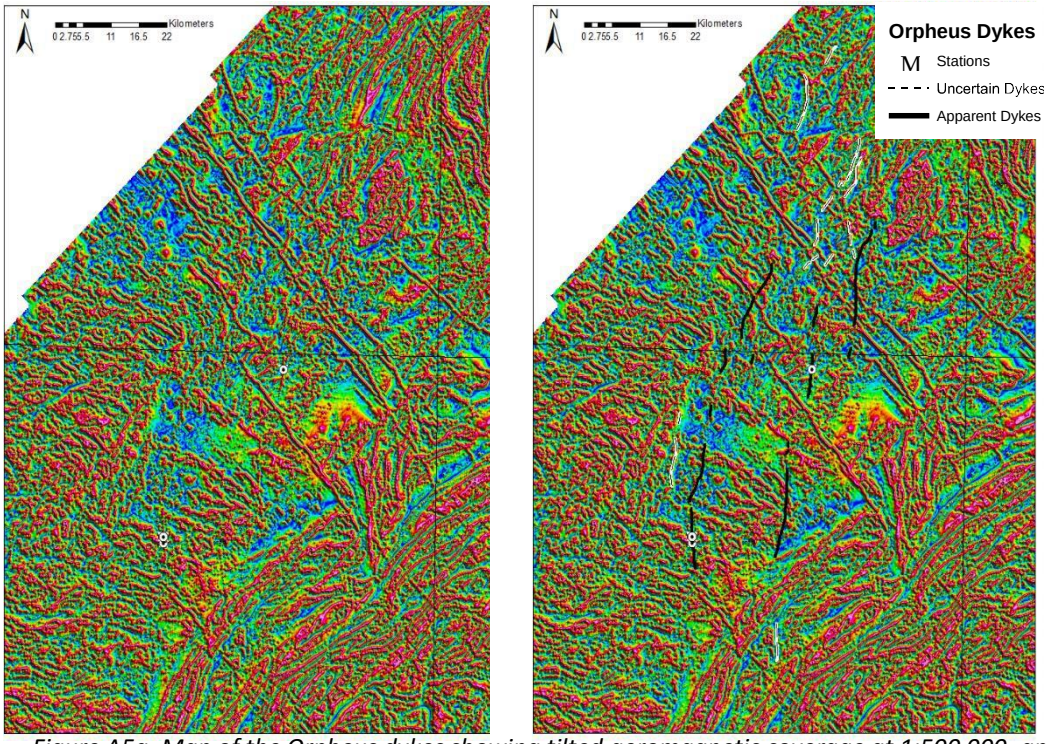

Figure A5a. Map of the Orpheus dykes showing tilted aeromagnetic coverage at 1:500 000, and A11b, right, with interpretation

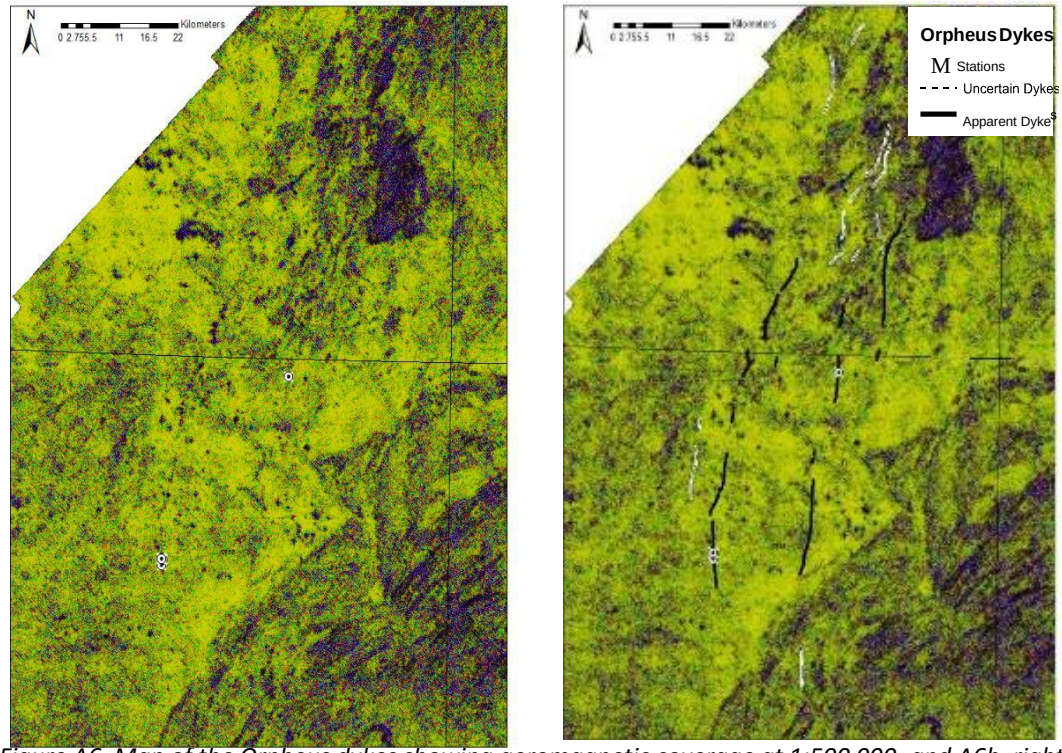

Figure A6. Map of the Orpheus dykes showing aeromagnetic coverage at 1:500 000, and A6b, right, with interpretation

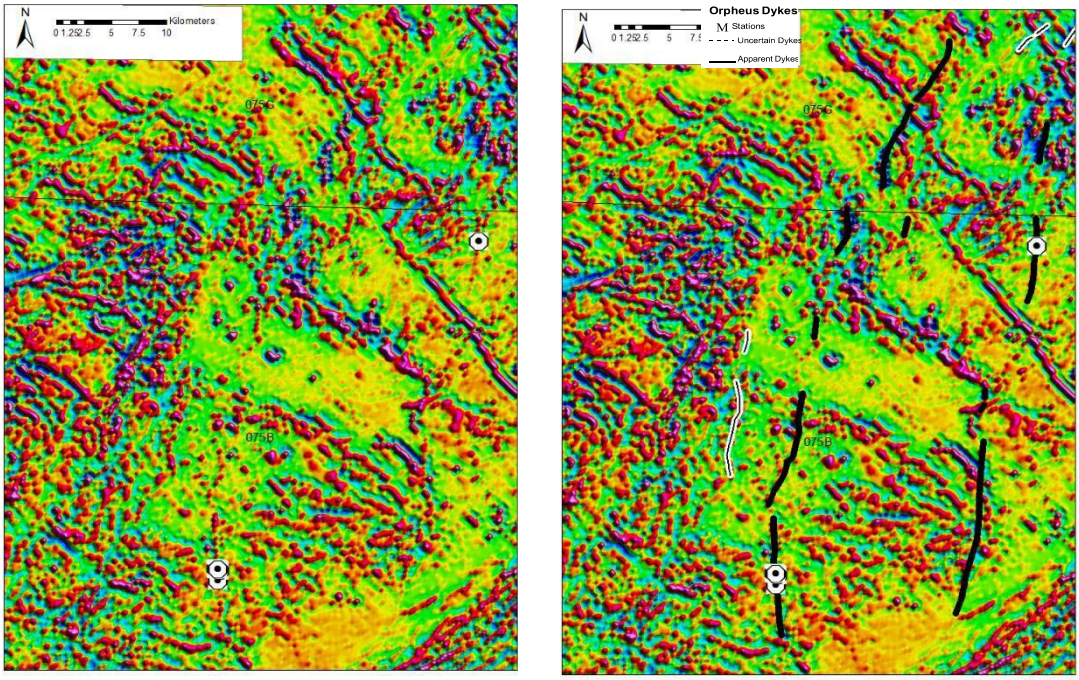

Figure A7a. Map of the Orpheus dykes showing first derivative aeromagnetic coverage at 1:250 000, and A7b, right, with interpretation

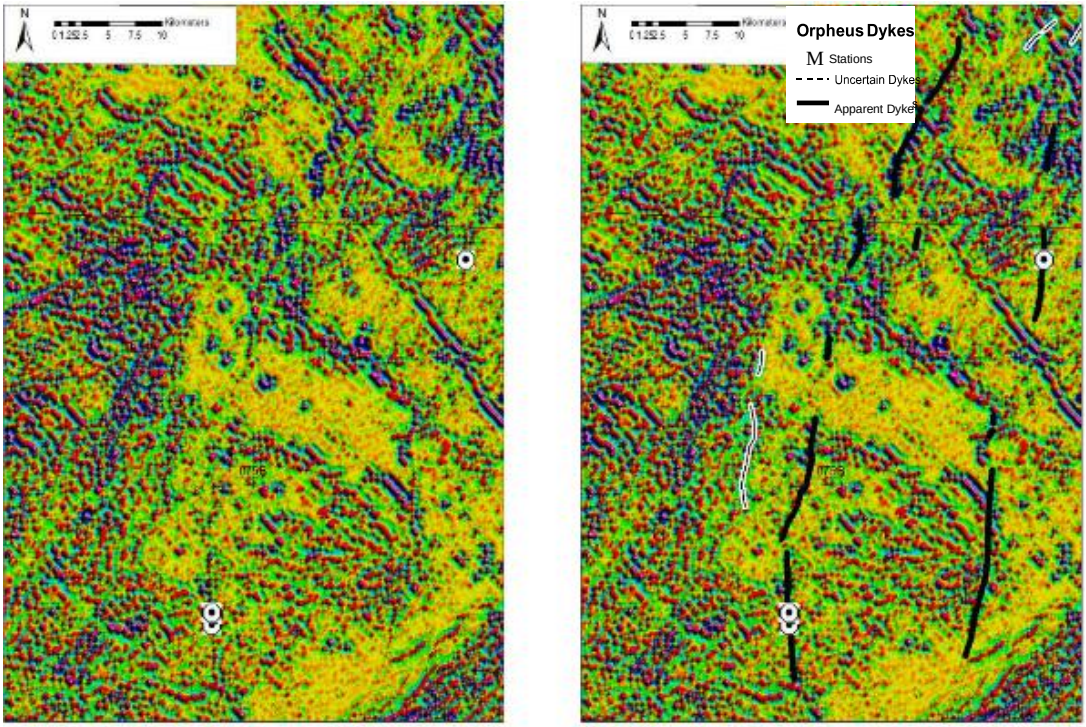

Figure A8a. Map of the Orpheus dykes showing second derivative aeromagnetic coverage at 1:250 000, and A8b, right, with interpretation

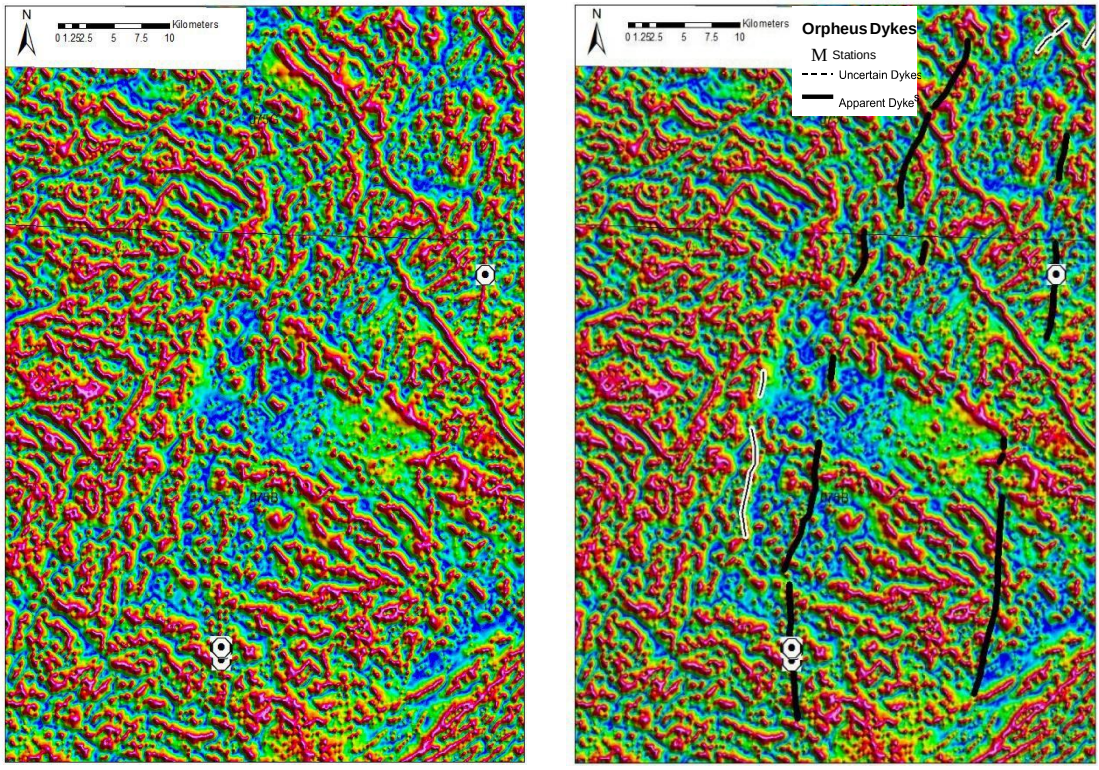

Figure *A9a, left. Map of the Orpheus dykes showing tilted aeromagnetic coverage at 1:250 000, and A9b, right, with interpretation*

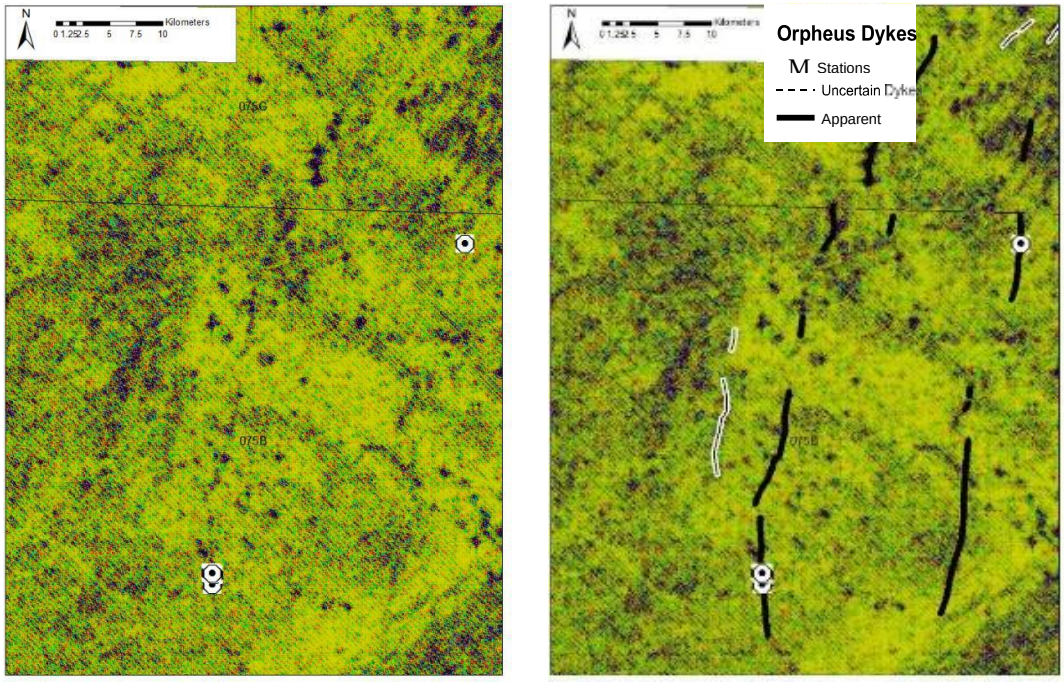

Figure A10a. Map of the Orpheus dykes showing aeromagnetic coverage at 1:250 000, and A10b, right, with interpretation

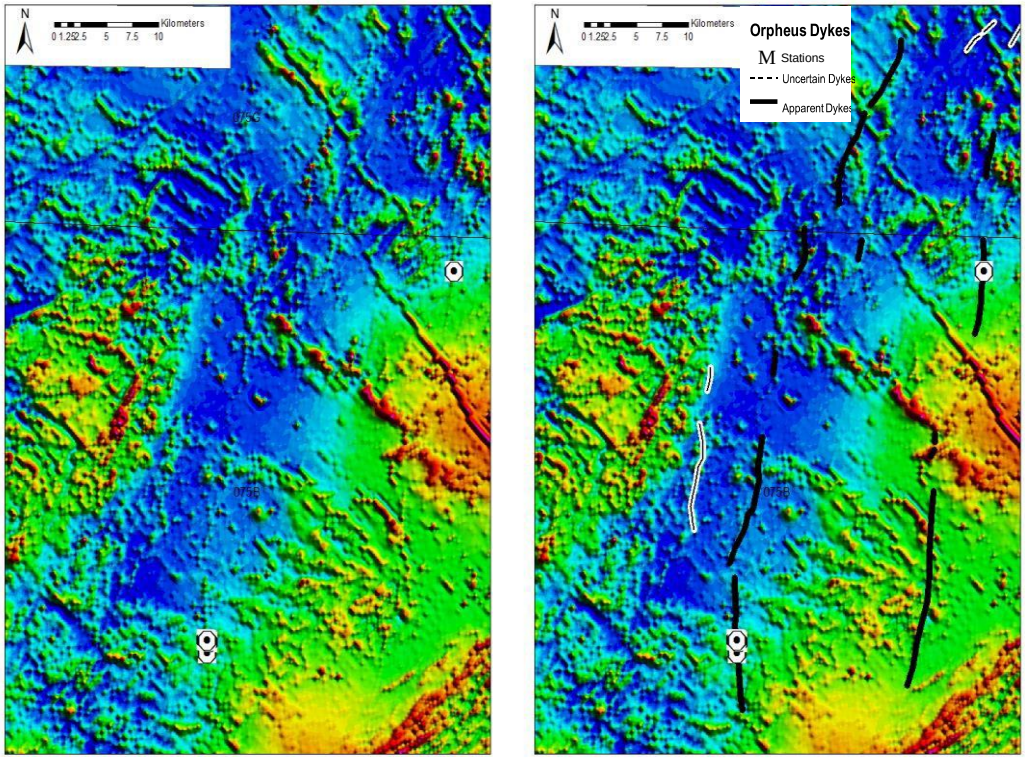

Figure A11a. Map of the Orpheus dykes showing aeromagnetic coverage at 1:250 000, and A11b, right, with interpretation

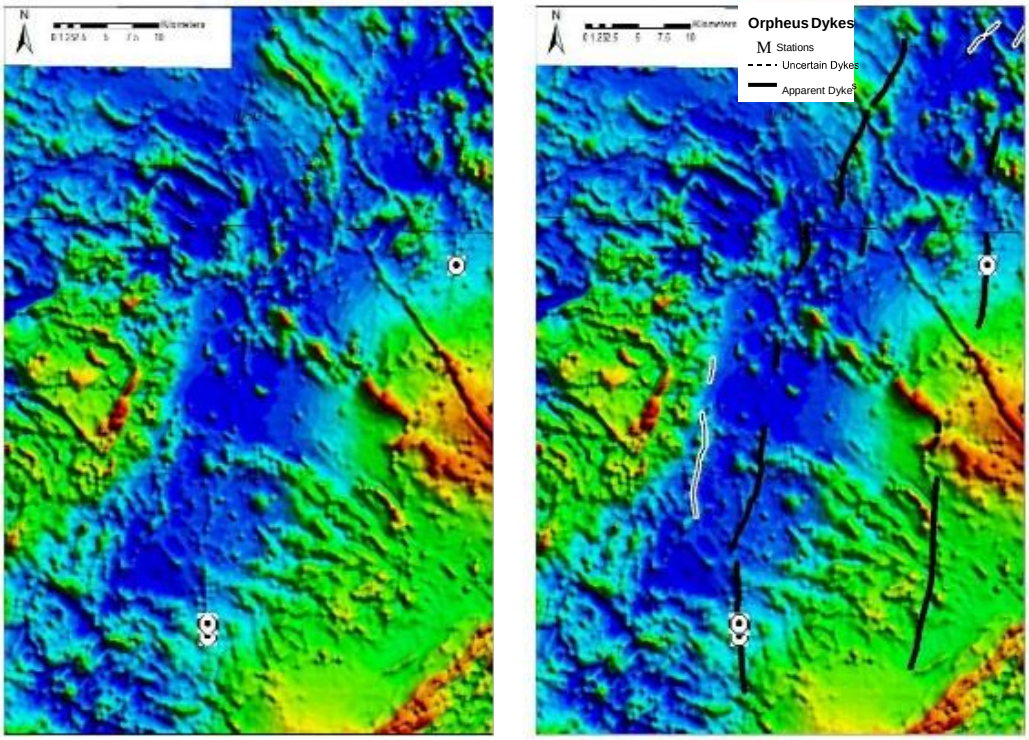

Figure A12a. Map of the Orpheus dykes showing aeromagnetic coverage at 1:250 000, and A12b, right, with interpretation